



Crystal Structure Elucidation of the Novel Molecular-Inorganic Polymer $K_2SeO_4 \cdot H_2SeO_3$.

Oscar S. Hernández-Daguer ^{1,2}, Charles L. Barnes³, Samuel P. Hernández-Rivera⁴, and Jorge L. Ríos-Steiner ⁵

¹*Department of Physics, University of Massachusetts, Amherst, Massachusetts 01003, United States, e-mail: ohernandezda@umass.edu, oscarsaidh@gmail.com*

²*Department of Physics, University of Puerto Rico, Mayagüez, Puerto Rico 00681-9000, United States, e-mail: oscar.hernandez3@upr.edu, oscarsaidh@gmail.com, phone: +1 787 228 1380.*

³*Department of Chemistry, University of Missouri, Columbia, Missouri 65211, United States.*

⁴*ALERT-II DHS Center of Excellence for Explosives Research, Department of Chemistry, University of Puerto Rico, Mayagüez, Puerto Rico, 00681-9000, United States.*

⁵*Laboratory of Crystallography and Synthesis of New Materials, Department of Chemistry, University of Puerto Rico, Mayagüez, Puerto Rico, 00681-9000 United States, e-mail: jorge.rios2@upr.edu, phone: +1 787 832 4040 ext 2538, Fax: +1 787 265 3849.*

January 15, 2019

Abstract

The orthorhombic crystal structure of the novel molecular-inorganic polymer $K_2SeO_4 \cdot H_2SeO_3$ was elucidated using single-crystal X-ray diffraction with $MoK\alpha$ radiation ($\lambda = 0.71073 \text{ \AA}$), performed at 100 and 298.15 K. The reported data is at 100 K since there were no structural differences as compared to the room temperature. The technique revealed $K_2SeO_4 \cdot H_2SeO_3$ crystals to have space group $Pbcm$ with unit cell dimensions $a = 8.8672(17) \text{ \AA}$, $b = 7.3355(14) \text{ \AA}$, $c = 11.999(2) \text{ \AA}$ and $Z = 4$. The unit cell volume obtained was $V = 780.5(3) \text{ \AA}^3$ with a calculated density $D_c = 2.980 \text{ Mg/m}^3$. In $K_2SeO_4 \cdot H_2SeO_3$, the selenate anions and selenous acid molecules form an infinite polymeric chain along the c axis, through strong hydrogen bonds. That

is to say; there are two distinctive species forming a polymeric sequence extended along the c axis with an alternating molecule-anion-molecule $(\text{SeO}_4^{2-} - \text{H}_2\text{SeO}_3)_n$, defined as a Molecular Inorganic Polymer (MIP). The K^+ cations influence the orientation of the SeO_4^{2-} anions, and these consequently affect the arrangement of the H_2SeO_3 molecules within the structure. The crystal packing forces are governed by ionic and dipole-dipole interaction. Full-matrix least-square refinement method on F^2 provide final Reliability indices of $R_1 = 0.0150$, and $wR_2 = 0.0377$, and a Goodness-of-fit = 1.140; at 0.75 Å resolution, where $R_{int} = 0.0230$, and $F(000) = 656$ for 1014 independent reflections ($I > 2\sigma(I)$), from a total of 8,576 reflections collected. Based on the crystallographic similarities of this novel structure with other previously reported compounds, potential non-linear optical, fast-proton conduction and acid transporting host material properties can be expected to develop solid-state technological applications with this crystal.

Keywords: Molecular Inorganic Polymer, $\text{K}_2\text{SeO}_4 \cdot \text{H}_2\text{SeO}_3$, Crystal Structure, Fuel cells.

1 Introduction

The coupling of these two intricate and concerning issues, global warming [1–4](that is requiring drastic actions [1])and the energy crisis [5, 6], have motivated the direction of most research efforts towards the development of alternative energy sources. The efforts to develop these alternatives [7, 8] and the development of materials with high ionic conduction, also known as Superionic Conductors, have encouraged scientists to study materials with high ionic conductive properties. Since the 1970s, study in this field has developed rapidly [9], mainly due to the potential applications in fuel cell technology. Fuel cells are electrochemical devices that use electrolytes to produce electricity. It has become an energy alternative (along with solar energy) since it generates electricity with high efficiency by combining hydrogen and oxygen electrochemically without combustion, producing water and heat as by-products [10].

Polymer electrolyte membranes (PEM) are currently considered the most adequate for the construction of portable fuel cells, making it ideal for automotive applications, like cars [11–13], trains [14–16] and aircraft [17–19]. These PEM Fuel cells (PEMFCs) have many advantages, such as rapid starting time, high energy efficiency and compactness, among others. Despite this, membranes require the continuous addition of water to transfer the protons

through the electrolyte solution and also require platinum to catalyze the oxidation of H_2 and the reduction of O_2 [11] this restricts the membranes to have to operate below the boiling point of water, the temperature range at which precious-metal catalysts work slowly and can become inactivated by the binding of carbon monoxide [13]. Different types of fuel cells have been proposed to overcome these issues, such as Alkaline Fuel Cells (AFCs) [20], Protonic Ceramic Fuel Cells (PCFCs) [21], and one of the most studied, solid Acid Fuel Cells (SAFCs) [13].

The evidence of a superprotonic phase in solid acid salts, such as in the family of $MHAO_4$, $M_3H(AO_4)_2$, $M_4H_2(AO_4)_3$, $M_5H_7(RO_4)_4$, $M_5H_3(AO_4)_4 \cdot xH_2O$, $M_9H_7(AO_4)_8 \cdot H_2O$ ($M = K^+$, Rb^+ , $(NH_4)^+$, Cs^+ ; $A = S, Se$), and MH_2RO_4 ($R = P, As$) [22–24] and other compounds created based on these proton conductor families [25–40], opens the possibility for a wider range of temperatures in which the fuel cells operate (outside the temperature range in which the water is liquid, assuming that materials with a superprotonic phase would be developed below $0^\circ C$). In addition, these solid acid electrolytes might reduce manufacturing costs by eliminating the use of platinum as a catalyst, without disregarding the possibility for yields and lifetime increases for these devices [8]. Compounds of the $M_3X(AO_4)_2$ family [41, 42], such as $K_3H(SeO_4)_2$, $Rb_3H(SeO_4)_2$, $(NH_4)_3H(SeO_4)_2$, etc., possess high proton conductivity and have been broadly reported to have a superionic phase transition above $112^\circ C$ [42–46], encouraging the design of fuel cells that operate at temperatures above the normal boiling point of water. However, some inconsistencies have been found in the thermal and electrical behavior of members of the $M_3X(AO_4)_2$ family [44, 47–50] and other families mentioned above. Due to these inconsistencies, different physical and chemical points of view have attempted to explain the process that produces the fast ion conduction in $M_3X(AO_4)_2$ acid salts [42, 43, 46, 49, 51–70], as is the case of $K_3H(SeO_4)_2$ (abbreviated as TKHSe). The superionic phase transition in TKHSe has been observed around T_p ($114^\circ C$) by performing thermal and electrical studies under different experimental tests and conditions. The results published by different authors reflect discrepancies in the superionic phase transition temperature T_p values. Values have been reported in the range between $108.1^\circ C$ and $122^\circ C$ [?, ?, ?, 49]. A recent report [71] claims that TKHSe undergoes a phase transition at around $112^\circ C$ and simultaneously decomposes in the temperature range of 110 to $150^\circ C$, starting at the surface of the TKHSe grains. The assumption is that the decomposition is analogous to that reported by Lee [72], for the KDP-type crystals, which suggest that the observed decrease in conductivity on successive thermal runs is a consequence of thermal decomposition (thermally activated). However, the jump in conductivity is only a consequence of the order-disorder transition in the TKHSe

phase that remains inside the grains. This implies that TKHSe cannot fulfill the electrical and thermal requirements to be applied in fuel cells; due to thermal instability in its superprotonic phase. O.S. Hernández-Daguer et al. [71], presumes that through variations in the atomic proportions in the $M_3H(AO_4)_2$ family, that is, by increasing the amount of selenate tetrahedra, one could possibly generate new chemical structures and materials that preserve the electrical properties and lack the thermal instability present in $K_3H(SeO_4)_2$ (analogous to thermal stability profiles present in ceramic materials [73]). Based on this hypothesis and looking for the superionic phase transition temperatures of the $M_4H_2(AO_4)_3$ family [74, 75, 75–79], we were able to synthesize a novel compound, $K_2SeO_4 \cdot H_2SeO_3$. The chemical structure of this compound was determined by single crystal X-ray diffraction.

2 Experimental

In order to synthesize some selenic acid salts, one of the products obtained was a novel compound, identified using single crystal X-ray diffraction and selected for our studies. Single crystals of the new compound were selected under a polarizing microscope (for size and optical quality selection purposes) in order to avoid multiple aggregates, twinned crystals and to improve diffraction quality) and recovered with paratone oil, to avoid the hydration of the crystals, and mounted on a Metegen micropin. The chosen crystals were 100 to 500 μm in size. Diffraction data for the novel compound was collected at 293K and at 100K with a Bruker diffractometer equipped with a graphite monochromator using $\text{MoK}\alpha$ radiation ($\lambda = 0.71073 \text{ \AA}$). This equipment is also coupled to an APEX II CCD area detector system and an Oxford Cryostream Low Temperature device. Data was collected using the ω and ϕ scan techniques. The structure and data collected at low temperature is the only one that will be reported since no significant structural differences were observed when compared to the room temperature structure. The temperature factors data is also better at low temperature, since the atoms are more localized due to less vibration in the crystal, which also improve the intensities and shape of the spots. Preliminary orientation matrixes (orientation matrix that specifies the orientation of the crystal and detector with respect to the X-ray beam), and unit cell parameters were obtained from ϕ and ω scans between $0^\circ \leq \phi \leq 90^\circ$, $20^\circ \leq \omega \leq 70^\circ$ and then refined using the whole data set. Frames were integrated and corrected for Lorentz and polarization effects. Equivalent reflections were merged, and absorption corrections were made using an empirical absorption methods [80], with $T_{\text{min}} = 0.11$ and $T_{\text{max}} = 0.33$ (Max. and Min. transmission). Space group, lattice

parameters and other relevant information are listed in Table 1.

The structure was solved by direct methods and refined by fullmatrix least-squares on $|F|^2$ (SHELX 97 program [81]), with the aid of the program X-SEED [82]. Anisotropic thermal factors were assigned to all the non-hydrogen atoms. All the hydrogen atoms were located in the $F_o - F_c$ map and refined accordingly. The fullmatrix least-squares method minimizes the function $w(F_o - F_c)^2$, where w represents the weight to be assigned an observation, associated to this discrepancies between the observed and calculated values of F 's (or $|F|^2$). The final refined atomic parameters are given in Table 2.

Table 1: Crystal data and structure refinement parameters for $\text{K}_2\text{SeO}_4 \cdot \text{H}_2\text{SeO}_3$

Identification code	$\text{K}_2\text{SeO}_4 \cdot \text{H}_2\text{SeO}_3$	
Empirical formula	$\text{H}_2\text{K}_2\text{O}_7\text{Se}_2$	
Formula weight	350.14	
Temperature	100(2) K	
Wavelength	0.71073 Å	
Crystal system	Orthorhombic	
Space group	$Pbcm(N^\circ 57)$	
Unit cell dimensions	$a = 8.8672(17)$ Å	$\alpha = 90^\circ$
	$b = 7.3355(14)$ Å	$\beta = 90^\circ$
	$c = 11.999(2)$ Å	$\gamma = 90^\circ$
Volume	$780.5(3)$ Å ³	
Z	4	
Density (calculated)	2.980 Mg/m ³	
Absorption coefficient	10.532 mm ⁻¹	
$F(000)$	656	
Crystal size	0.500 x 0.250 x 0.200 mm ³	
Theta range for data collection	$2.297^\circ \leq \theta \leq 28.676^\circ$.	
Index ranges	$-11 \leq h \leq 11,$ $-9 \leq k \leq 9,$ $-15 \leq l \leq 16$	
Reflections collected	8576	
Independent reflections	1014 [$R_{(int)} = 0.0230$]	
Completeness to theta = 25.242°	100.0 %	
Absorption correction	Semi-empirical from equivalents	
Max. and min. transmission	0.23 and 0.11	
Refinement method	Full-matrix least-squares on F^2	
Data / restraints / parameters	1014 / 0 / 61	
Goodness-of-fit on F^2	1.140	
Final R indices [$I > 2\sigma(I)$]	$R_1 = 0.0150, wR_2 = 0.0377$	
R indices (all data)	$R_1 = 0.0159, wR_2 = 0.0380$	
Extinction coefficient	0.0093(4)	
Largest diff. peak and hole	0.575 and -0.458 e.Å ⁻³	

Table 2: Atomic coordinates ($\times 10^4$) and equivalent isotropic displacement parameters ($\text{\AA}^2 \times 10^3$) for $\text{K}_2\text{SeO}_4 \cdot \text{H}_2\text{SeO}_3$. $U_{(eq)}$ is defined as one third of the trace of the orthogonalized U_{ij} tensor.

	x	y	z	$U_{(eq)}$
Se(1)	8184(1)	7500	5000	8(1)
Se(2)	3742(1)	5921(1)	2500	11(1)
K(1)	7938(1)	2500	5000	11(1)
K(2)	10728(1)	4584(1)	7500	10(1)
O(1)	7132(2)	5928(2)	4401(1)	16(1)
O(2)	9236(2)	6548(2)	5952(1)	14(1)
O(3)	4574(2)	7086(2)	3610(1)	16(1)
O(4)	2121(2)	6974(3)	2500	12(1)

3 Results and Discussion

Figure 1 displays a visualization of two different views of the suitable trial structures model found for the crystal structure at $\text{K}_2\text{SeO}_4 \cdot \text{H}_2\text{SeO}_3$, which is a projection on ac plane. The dotted lines in the figure represent hydrogen bonds and solid lines indicate covalent bonding. The ellipsoids (so called thermal ellipsoids) in Figure 1 show the amount by which atoms are displaced in a given direction (showed by the shape of the ellipsoid, a cigar shape indicating much motion or displacement). And also indicates the direction of maximum motion [83]. The $\text{K}_2\text{SeO}_4 \cdot \text{H}_2\text{SeO}_3$ crystal is built of potassium cation environments, selenate anions and molecules of selenous acid, similar to $\text{Na}_2\text{SeO}_4 \cdot \text{H}_2\text{SeO}_3 \cdot \text{H}_2\text{O}$ [84]. The structure consists of slightly distorted tetrahedron SeO_4^{2-} anions, electrically equilibrated by K^+ cations, and joined by hydrogen bonds with an almost regular pyramidal SeO_3 anion to form a double sequence of anion-molecule-anion extending parallel to the c axis, see Figure 1.

The crystals of $\text{K}_2\text{SeO}_4 \cdot \text{H}_2\text{SeO}_3$ have two types of K cations (See Figure 2 and Table 3): K(1) occupies special positions and is surrounded by ten oxygen atoms, see Figure 2 a, of which eight are coordinated to it. Two of them are at a longer distance, 3.3835 \AA , but they seem to be part of the environment of K(1). K(2) is at a general position and is coordinated to eight oxygen atoms (Figure 2 b).

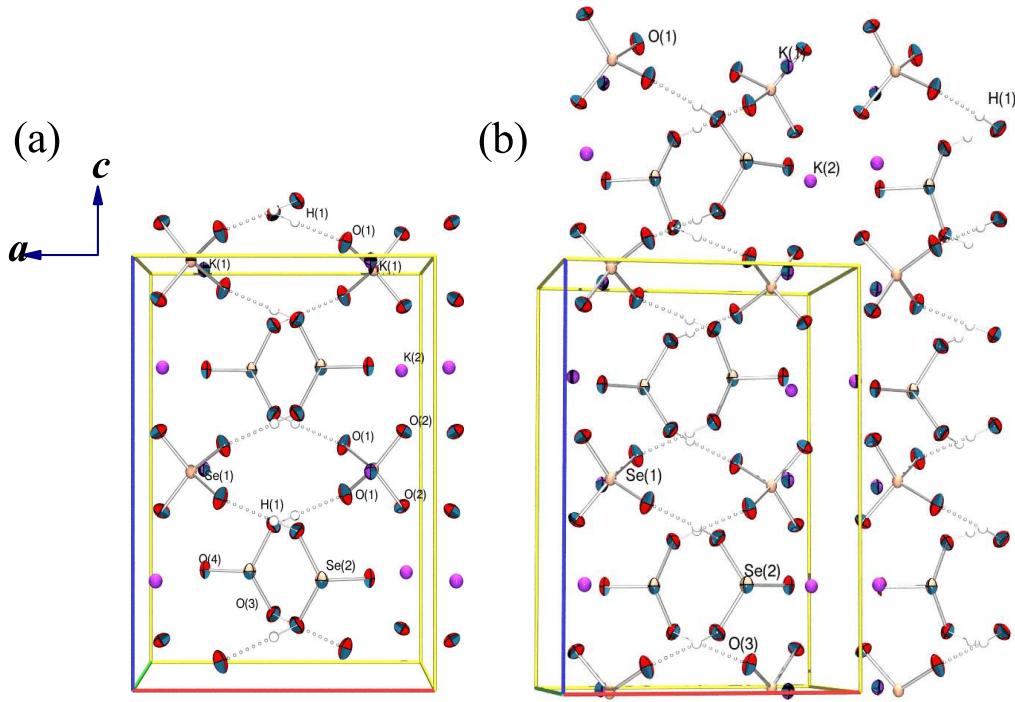


Figure 1: The crystal structure of $K_2SeO_4 \cdot H_2SeO_3$ at 100K. (a) Projection of the crystal structure onto the ac plane or (010). (b) Clinographic projection of the structure. The dot lines in the figure represent the hydrogen bonds. The figure was generated with the crystal structure visualization program Ortep III [85] and with the aid of the program POV-Ray [86].

Table 3: Potassium-oxygen interatomic bonds distances, in $K_2SeO_4 \cdot H_2SeO_3$ crystal structure.

Bond	Distance (Å)	Bond	Distance (Å)
K(1)-O(1) ^{#8}	2.7109(15)	K(2)-O(2)	2.6977(14)
K(1)-O(1)	2.7109(15)	K(2)-O(2) ^{#11}	2.6977(14)
K(1)-O(3) ^{#9}	2.7987(16)	K(2)-O(4) ^{#7}	2.773(2)
K(1)-O(3) ^{#7}	2.7987(16)	K(2)-O(4) ^{#12}	2.811(2)
K(1)-O(2) ^{#10}	2.8409(16)	K(2)-O(2) ^{#10}	2.9002(15)
K(1)-O(2) ^{#2}	2.8409(16)	K(2)-O(2) ^{#13}	2.9002(15)
K(1)-O(4) ^{#9}	3.0248(6)	K(2)-O(1) ^{#14}	2.9907(16)
K(1)-O(4) ^{#7}	3.0248(6)	K(2)-O(1) ^{#2}	2.9907(16)
K(1)-O(2) ^{#8}	3.3834(15)	Average	2.8451
K(1)-O(2)	3.3835(15)		
Average	2.9517		

^{#2}: $-x+2, -y+1, -z+1$ ^{#7}: $-x+1, -y+1, -z+1$ ^{#8}: $x, -y+1/2, -z+1$ ^{#9}:
 $-x+1, y-1/2, z$ ^{#10}: $-x+2, y-1/2, z$ ^{#11}: $x, y, -z+3/2$ ^{#12}: $x+1, -y+3/2, -z+1$ ^{#13}:
 $-x+2, y-1/2, -z+3/2$ ^{#14}: $-x+2, -y+1, z+1/2$

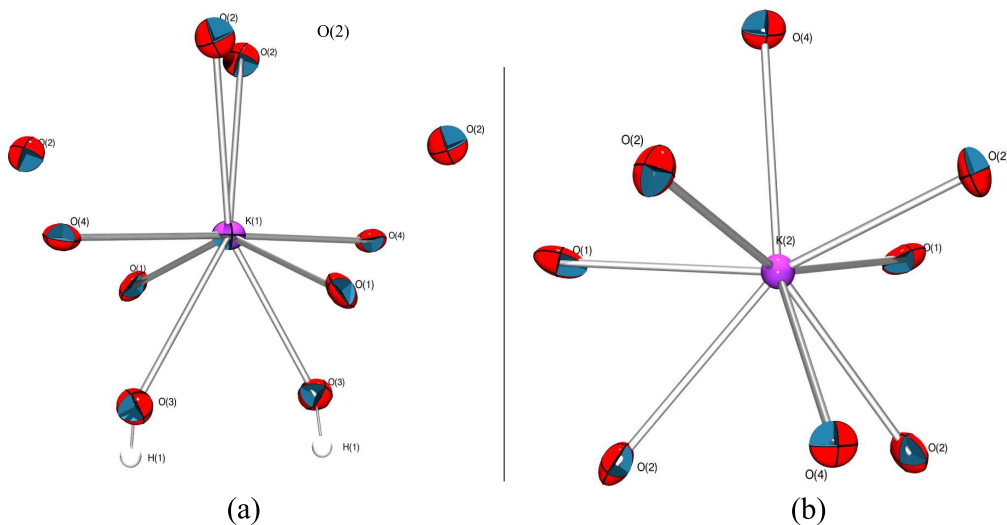


Figure 2: The potassium atoms environment. (a) Oxygen atoms surrounding K(1) and (b) oxygen atoms around K(2). The figure was generated with the crystal structure visualization program Ortep III [85] and with the aid of the program POV-Ray [86].

However, both types of potassium atoms have *eight* oxygen atoms as their nearest neighbors, with an average potassium-oxygen distance of 2.8438 and 2.8451 Å for K(1) and K(2) respectively. Including all oxygen atoms surrounding the potassium atoms the average potassium-oxygen distance are 2.9517 Å for K(1) and 2.8451 Å for K(2), unlike the average distances and the number of surroundings oxygen atoms reported for K_2SeO_4 [87], with average values of 3.14 Å for K(1) and 2.93 Å for K(2). The Se(1) is at a special position and Se(2) occupies a general position (Table 2 and Figure 1). The crystal packing shows selenate anions and selenous acid molecules form an infinite polymeric chain of alternating species along the c axis, mediated by strong hydrogen bonds, salt bridges and ion-dipole interactions [88]. In other words, $(\text{SeO}_4^{2-} - \text{H}_2\text{SeO}_3)_n$, defined as a *Molecular Inorganic Polymer* (MIP), see Figure 3a, seems to resemble the selenous acid crystal structure [89] as shown in Figure 3. The H_2SeO_3 and SeO_4^{2-} anions, in $\text{K}_2\text{SeO}_4 \cdot \text{H}_2\text{SeO}_3$ crystal structure, are oriented towards the K^+ ions. The K^+ ions, with their electrical charge, influence the orientation of the SeO_4^{2-} anions and these consequently affect the arrangement of the H_2SeO_3 molecules within the structure.

The selenate anions participate in two hydrogen bonds as a proton acceptor through the symmetry-equivalent O(1) and O(3) oxygens. Due to

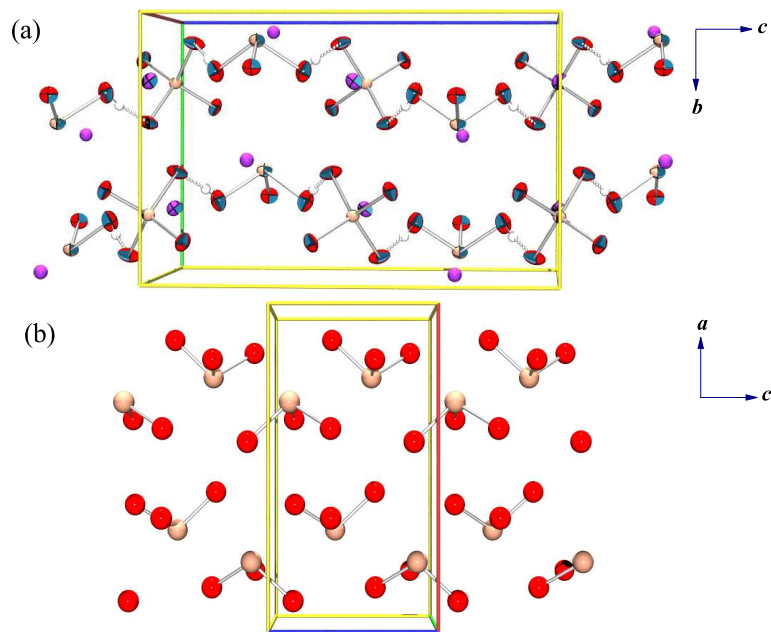


Figure 3: Representation of: (a) polymeric anion-molecule-anion $(\text{SeO}_4 - \text{H}_2\text{SeO}_3)_n$ sequence, projected onto the bc plane for $\text{K}_2\text{SeO}_4 \cdot \text{H}_2\text{SeO}_3$ crystal structure. (b) sequence $(\text{H}_2\text{SeO}_3 - \text{H}_2\text{SeO}_3)$ onto the ac plane [89]. The figure was generated with the crystal structure visualization program Ortep III [85] and with the aid of the program POV-Ray [86].

this, the $\text{Se}(1)\text{-O}(1)$ and $\text{Se}(1)\text{-O}(1)\#1$ bonds ($1.6484(13) \text{ \AA}$) are longer than the two remaining $\text{Se}(1)\text{-O}(2)$ and $\text{Se}(1)\text{-O}(2)\#1$ ($1.6319(13) \text{ \AA}$), as shown in Table 4 and Figure 4.

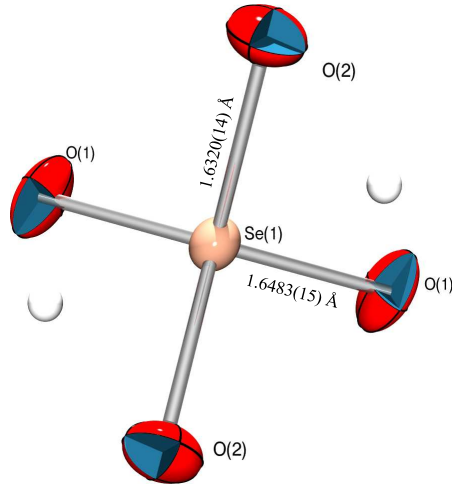


Figure 4: Selenium-oxygen interatomic bond distances for the SeO_4^{2-} anions, in $\text{K}_2\text{SeO}_4 \cdot \text{H}_2\text{SeO}_3$ crystal structure. The figure was generated with the crystal structure visualization program Ortep III [85] and with the aid of the program POV-Ray [86].

Table 4: Selenium-oxygen interatomic bond distances and angles for the SeO_4^{2-} anions, in $\text{K}_2\text{SeO}_4 \cdot \text{H}_2\text{SeO}_3$ crystal structure.

Bond	Distance (Å)	Bond angle	Angle (°)
Se(1)-O(2) ^{#1}	1.6319(13)	O(2) ^{#1} -Se(1)-O(2)	110.22(10)
Se(1)-O(2)	1.6319(13)	O(2) ^{#1} -Se(1)-O(1) ^{#1}	109.23(7)
Se(1)-O(1) ^{#1}	1.6484(13)	O(2)-Se(1)-O(1) ^{#1}	108.54(7)
Se(1)-O(1)	1.6484(13)	O(2) ^{#1} -Se(1)-O(1)	108.54(7)
Average	1.6401	O(2)-Se(1)-O(1)	109.23(7)
		O(1) ^{#1} -Se(1)-O(1)	111.08(10)
		Average	109.47
O(1)-O(2) ^{#1}	2.663(2)		
O(2)-O(1)	2.674(3)		
O(1) ^{#1} -O(1)	2.718(3)		
O(2) ^{#1} -O(2)	2.663(2)		
O(1) ^{#1} -O(1) ^{#1}	2.674(3)		

^{#1} : x,-y+3/2,-z+1

The selenate oxygen atoms that are acting as hydrogen bond acceptors have longer Se(1)-O(1) bonds distances compared to those that are not participating in the hydrogen bond scheme, due to the electron density withdrawing

effect of the H-bond formation. The hydrogens decrease the charge density of the oxygen involved in the interaction, weakening the Se(1)-O(1) bonds. The O-Se(1)-O bonds angles, listed in Table 4; are not significantly different, forming a little bit of a distorted tetrahedron (almost regular tetrahedron). The mean value Se-O distance is 1.6401 Å which is in good agreement with the average for selenate anions in some crystals member of Me_2SeO_4 family [87, 90].

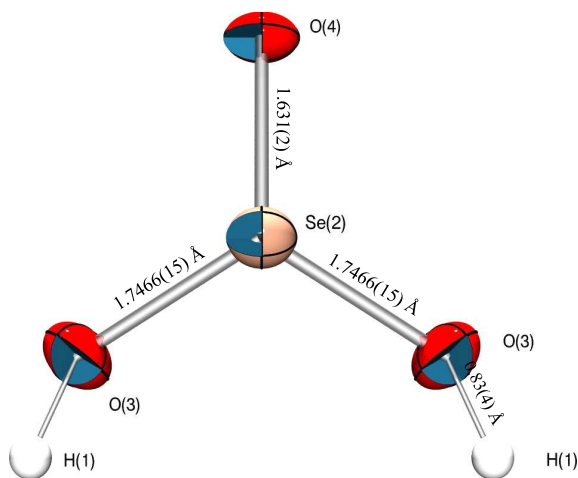


Figure 5: Selenium-oxygen interatomic bond distances and angles for the H_2SeO_3 molecule, in $\text{K}_2\text{SeO}_4 \cdot \text{H}_2\text{SeO}_3$ crystal structure. The figure was generated with the crystal structure visualization program Ortep III [85] and with the aid of the program POV-Ray [86].

The structure arrangement of H_2SeO_3 molecules (see Figure 5), is listed in Table 5, the molecule displays an almost regular pyramidal units, joined to hydrogen atoms where the average O-Se-O angle is 98.53° .

Table 5: Selenium-oxygen interatomic bond distances and angles for the H_2SeO_3 molecule, in $\text{K}_2\text{SeO}_4 \cdot \text{H}_2\text{SeO}_3$ crystal structure at 100 K.

Bond	Distance (Å)	Bond angle	Angle (°)
Se(2)-O(4)	1.6311(19)	O(4)-Se(2)-O(3)	98.08(7)
Se(2)-O(3)	1.7466(15)	O(4)-Se(2)-O(3) ^{#5}	98.08(7)
Se(2)-O(3) ^{#5}	1.7467(15)	O(3)-Se(2)-O(3) ^{#5}	99.43(10)
		Average	98.53
O(3)-H(1)	0.83(3)	Se(2)-O(3)-H(1)	115(2)
O(4)-O(3)	2.552(3)		
O(4)-O(3) ^{#5}	2.552(3)		
O(3)-O(3) ^{#5}	2.665(3)		

^{#5}: x,y,-z+1/2

The distances observed in our structure, resembles the very closely those of the crystal of selenous acid, as those reported by F. Larsen [91]. The selenium-oxygen distances can be classified in two different categories (see the second column of Table 5): the hydroxyl-oxygens and non-hydroxyl ones. Here, the hydroxyl-oxygens have a longer distance to Se(2), when compared to the non-hydroxyl ones. With Se(2)-O(4) distances of 1.631 Å and Se(2)-O(3) distances of 1.746 Å. The differences between Se-O(3) and Se-O(4) distances is 0.1156 Å. The O-H distance is 0.83(3) Å, a short distance than that reported for H_2SeO_3 [91], $\beta\text{-H}_2\text{SeO}_3$ [92] and $\text{Na}_2\text{SeO}_4 \cdot \text{H}_2\text{SeO}_3 \cdot \text{H}_2\text{O}$ crystals [84].

Table 6: Hydrogen bonds in $\text{K}_2\text{SeO}_4 \cdot \text{H}_2\text{SeO}_3$ crystal structure at 100 K.

D-H...A	d(D-H) (Å)	d(H...A) (Å)	d(D...A) (Å)	Angle<(DHA)(°)
O(3)-H(1)... Se(1)	0.83(3)	2.93(3)	3.6215(15)	142(3)
O(3)-H(1)... O(1)	0.83(3)	1.78(3)	2.601(2)	171(3)

Table 7: Hydrogen coordinates ($\times 10^4$) and isotropic displacement parameters ($\text{Å}^2 \times 10^3$) for $\text{K}_2\text{SeO}_4 \cdot \text{H}_2\text{SeO}_3$. $U_{(eq)}$ is defined as one third of the trace of the orthogonalized U_{ij} tensor. The figure was generated with the crystal structure visualization program Ortep III [85] and with the aid of the program POV-Ray [86].

	x	y	z	$U_{(eq)}$
H(1)	5350(40)	6610(50)	3860(30)	45(9)

The molecule of selenous acid plays the role of a proton donor in two strong hydrogen bonds, through symmetry-equivalent O(3) and O(3)^{#5} oxy-

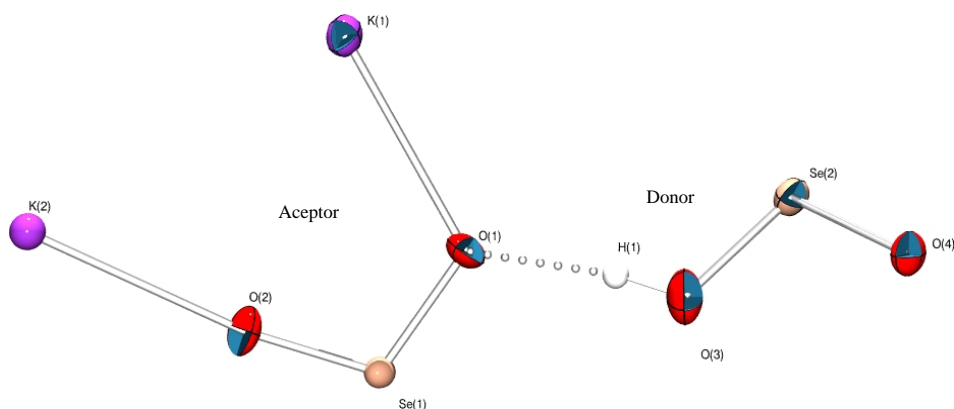


Figure 6: Show the asymmetric unit of $\text{K}_2\text{SeO}_4 \cdot \text{H}_2\text{SeO}_3$. The molecule of selenous acid H_2SeO_3 , at the right side, is labeled as Donor. The SeO_4^{2-} anions, at the left side is labeled as Acceptor. The figure was generated with the crystal structure visualization program Ortep III [85] and with the aid of the program POV-Ray [86].

gens with H(1), joined with O(1) and O(1)#1 oxygens bridging with its two neighbor SeO_4^{2-} anions (see Table 6, Table 7 and Figure 6).

3.1 Calculated X-ray powder diffraction information

The diffractogram of the novel structure $\text{K}_2\text{SeO}_4 \cdot \text{H}_2\text{SeO}_3$, described in the previous sections, is shown in Figure 7.

The Miller indices and associated parameters, related to the peaks show in Figure 7 for the $\text{K}_2\text{SeO}_4 \cdot \text{H}_2\text{SeO}_3$ crystal is shown in Table 8. These results are shown to facilitate the identification of the sample in future studies. In Figure 7, a plotted of the relative intensity vs. 2θ , in the range 15 to 35°, displays the calculated X-ray powder diffraction pattern, (generated with the Crystal Structure Visualisation Software Mercury [103]), of the of the compound $\text{K}_2\text{SeO}_4 \cdot \text{H}_2\text{SeO}_3$.

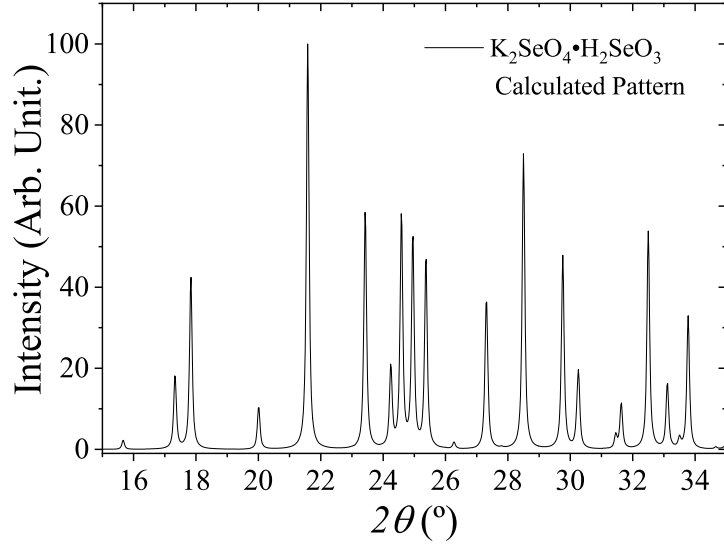


Figure 7: Calculated X-ray powder diffraction pattern for $\text{K}_2\text{SeO}_4 \cdot \text{H}_2\text{SeO}_3$.

Table 8: Miller indices and associated parameters, related to the peaks show in Figure 7 for the $\text{K}_2\text{SeO}_4 \cdot \text{H}_2\text{SeO}_3$ crystal^a. I : Intensity, I_{max} : Maximum intensity

2θ	I	$\frac{I}{I_{max}}$	d_{hkl} (d_{Bragg})	$\frac{1}{d^2}$	h	k	l	$\frac{1}{d_{Bragg}^2}$
15.66	222	2.22	5.668139035	0.031125692	1	1	0	0.031302297
17.32	1814	18.14	5.128455134	0.038021293	1	1	1	0.038247899
17.84	4241	42.41	4.980128375	0.040319852	1	0	2	0.040500647
20	1024	10.24	4.446893773	0.050569247	2	0	0	0.050872957
21.58	10000	100	4.12475581	0.058776472	1	1	2	0.059084705
23.42	5848	58.48	3.804699708	0.069081098	2	1	0	0.069457015
24.24	2106	21.06	3.677822022	0.073929638	0	2	0	0.074336233
24.58	5812	58.12	3.627715498	0.075985996	2	1	1	0.076402617
24.96	5250	52.5	3.573342227	0.07831605	2	0	2	0.078655365
25.38	4688	46.88	3.515155126	0.080930274	0	2	1	0.081281835
26.28	182	1.82	3.396783842	0.086669078	1	2	0	0.087054472
27.32	3634	36.34	3.269798405	0.093531531	1	1	3	0.093812715
28.5	7292	72.92	3.137049237	0.101614885	0	2	2	0.102118641
29.76	4790	47.9	3.007043171	0.110591226	0	0	4	0.111129632
30.26	1968	19.68	2.958488258	0.114251076	3	0	0	0.114464154
31.46	414	4.14	2.848329986	0.123259215	1	0	4	0.123847871
31.64	1147	11.47	2.832536221	0.124637594	2	2	0	0.12520919
32.5	5386	53.86	2.759524428	0.131320194	2	1	3	0.131967433
33.12	1621	16.21	2.709273027	0.136236806	0	2	3	0.136846651
33.5	352	3.52	2.679406659	0.139290897	3	1	1	0.139993814
33.78	3298	32.98	2.657836354	0.141560968	1	1	4	0.142431929
34.66	65	0.65	2.592348003	0.148803586	1	2	3	0.14956489

^a Crystal name: $\text{K}_2\text{SeO}_4 \cdot \text{H}_2\text{SeO}_3$, I_{max} : 10000, Unit Cell parameters: $a = 8.8672 \text{ \AA}$, $b = 7.3355 \text{ \AA}$, $c = 11.999 \text{ \AA}$, $\alpha = 90^\circ$, $\beta = 90^\circ$, $\gamma = 90^\circ$.

4 Conclusions

The structural arrangement of $\text{K}_2\text{SeO}_4 \cdot \text{H}_2\text{SeO}_3$ crystals resembles the selenous acid structure reported in the literature. Instead of having the sequence $(\text{H}_2\text{SeO}_3 - \text{H}_2\text{SeO}_3)_n$, the novel crystalline compound is formed by the alternating sequence molecule-anion-molecule $(\text{K}_2\text{SeO}_4 - \text{H}_2\text{SeO}_3)_n$, that is to say, the K_2SeO_4 replaces one of the H_2SeO_3 units. This pattern is possible, due to the electrical charge nature of both anions. In $\text{K}_2\text{SeO}_4 \cdot \text{H}_2\text{SeO}_3$, the charge of K^+ ions are balancing the ionic part of the structure while the hydrogen atoms are equilibrating the molecular part of the structure, see Figure 3.

Substantial differences were not observed in the interatomic distances present in the pyramidal units of SeO_3 in the H_2SeO_3 and $\beta\text{-H}_2\text{SeO}_3$ crystallographic structures and the corresponding unit present in this work. Unlike H_2SeO_3 , significant differences were found between the interatomic distances and chemical environment present in the K_2SeO_4 structure reported and the corresponding environment in the $\text{K}_2\text{SeO}_4 \cdot \text{H}_2\text{SeO}_3$ structure. These differences could be attributed to the type of interactions (ion-ion, ion-dipole) governing the crystal packing.

The chemical environment surrounding K(1) and K(2) ions, in the structure reported herein, are different. The potassium ion labelled K(1) has ten oxygen atoms in its neighborhood while K(2) has eight. However, both types of potassium atoms have eight oxygen atoms as their nearest neighbor, with an average potassium-oxygen distance of 2.8438 and 2.8451 Å, for K(1) and K(2) respectively.

The selenium-oxygen distance present in the SeO_4^{2-} anions and those in H_2SeO_3 can be classified into two groups, the ones where the hydrogen interacts and the ones where there are no interactions. Notice that in the selenate unit, the distances Se(1)-O(2) are slightly longer than the Se(1)-O(1), while in the selenous acid moiety, the Se(2)-O(3) distance is around 1 Å larger than the Se(2)-O(4). See Table 4, Table 5.

4.1 Future work

It seems plausible to study the $\text{K}_2\text{SeO}_4 \cdot \text{H}_2\text{SeO}_3$ crystals at above 299 K to see if a phase transition takes place, in the compound and analyze the physical and chemical properties of the crystals at room and higher temperatures, such as non-linear optical properties and fast-proton conductivity. One could do impedance spectroscopy measurements on the $\text{K}_2\text{SeO}_4 \cdot \text{H}_2\text{SeO}_3$ crystals to determine if it behaves as a solid state proton conductor. If it does, then it would be necessary to analyze the temperature dependence of proton con-

ductivity along the a , b and c axis to know if the conductivity is anisotropic, since the hydrogen bonding is extended along the c axis and one would expect to see higher proton conductivity. It is very likely that $\text{K}_2\text{SeO}_4 \cdot \text{H}_2\text{SeO}_3$ structure also behaves in a similar fashion to $\text{Na}_2\text{SeO}_4 \cdot \text{H}_2\text{SeO}_3 \cdot \text{H}_2\text{O}$, which generates efficient second harmonic radiation at 435.8 nm (blue region of the visible spectrum). This may require some empirical or semi-empirical calculation.

It is seeming reasonable to synthesize the $\text{M}_2\text{AO}_4 \cdot \text{H}_2\text{AO}_3$ and $\text{M}_3\text{RO}_4 \cdot \text{H}_3\text{RO}_3$ families ($\text{M} = \text{Li}^+, \text{Na}^+, \text{K}^+, \text{Rb}^+, (\text{NH}_4)^+, \text{Cs}^+$; $\text{A} = \text{S}, \text{Se}$, $\text{R} = \text{P}, \text{As}$), specially the $\text{K}_3\text{PO}_4 \cdot \text{H}_3\text{PO}_3$ and $\text{Cs}_3\text{PO}_4 \cdot \text{H}_3\text{PO}_3$ crystals, in order to study the new world of properties and possibilities that might arise in this tow families of compounds.

Many industrial applications require the use of selenous acid (H_2SeO_3) [93], such as, changing the color of steel, in particular the steel in guns, but it is difficult to transport it due to its high toxicity and corrosiveness. For this reason, it would be necessary to develop a method to separate the selenous acid from the K_2SeO_4 . These studies suggest that perhaps, it may be safer to transport H_2SeO_3 in the form of $\text{K}_2\text{SeO}_4 \cdot \text{H}_2\text{SeO}_3$, a polymeric crystal, instead of H_2SeO_3 alone.

5 Acknowledgement

Financial support of this work is acknowledged to the Center for Chemical Sensors Development at the Department of Chemistry, University of Puerto Rico-Mayagüez.

The authors thanks the Department of Chemistry, at the University of Missouri-Columbia for access to its instruments at the X-ray laboratory, for their technical assistance and expertise.

In addition, thanks to the College of Arts and Sciences of UPRM, and its Dean, Prof Manuel Valdés Pizzini, for providing the traveling and financial support for the Columbia, Missouri experience.

The authors to acknowledge the Department of Chemistry, UPR-Mayagüez for providing the access to X-ray facility. During the course of this investigation valuable insights and very helpful discussions with retired Prof. Oscar Rosado-Lojo took place, of which I am gratefully appreciative. We also thank the retired Prof. Rene S. Vieta for his encouragement and Sonai K. Donnell for her contribution in editing this document.

References

- [1] Jeff Tollefson. Clock ticking on climate action. *Nature*, 562(7726):172–173, oct 2018.
- [2] Nikolaos Christidis, Peter A. Stott, and Simon J. Brown. The Role of Human Activity in the Recent Warming of Extremely Warm Daytime Temperatures. *Journal of Climate*, 24(7):1922–1930, apr 2011.
- [3] Richard Monastersky. Climate crunch: A burden beyond bearing. *Nature*, 458(7242):1091–1094, apr 2009.
- [4] Svante Arrhenius. XXXI. On the influence of carbonic acid in the air upon the temperature of the ground. *The London, Edinburgh, and Dublin Philosophical Magazine and Journal of Science*, 41(251):237–276, apr 1896.
- [5] David E Newton. *World Energy Crisis: A Reference Handbook - ABC-CLIO*. ABC-CLIO Santa Barbara, California, 2012.
- [6] George F. Ray T. M. Rybczynski. *The Economics of the Oil Crisis*. Palgrave Macmillan UK, London, 1976.
- [7] Nikdalila Radenahmad, Ahmed Afif, Pg Iskandar Petra, Seikh M.H. Rahman, Sten-G. Eriksson, and Abul K. Azad. Proton-conducting electrolytes for direct methanol and direct urea fuel cells – A state-of-the-art review. *Renewable and Sustainable Energy Reviews*, 57:1347–1358, may 2016.
- [8] R. C. Agrawal and R. K. Gupta. Superionic solid: composite electrolyte phase – an overview. *Journal of Materials Science*, 34(6):1131–1162, 1999.
- [9] S HOSHINO. Structure and dynamics of solid state ionics. *Solid State Ionics*, 48(3-4):179–201, nov 1991.
- [10] Jeff Tollefson. Hydrogen vehicles: Fuel of the future? *Nature*, 464(7293):1262–1264, apr 2010.
- [11] P. D. Tran, A. Morozan, S. Archambault, J. Heidkamp, P. Chenevier, H. Dau, M. Fontecave, A. Martinent, B. Jusselme, and V. Artero. A noble metal-free proton-exchange membrane fuel cell based on bio-inspired molecular catalysts. *Chem. Sci.*, 6(3):2050–2053, feb 2015.

- [12] Yuyu Liu, Xiuping Yue, Kaixi Li, Jinli Qiao, David P. Wilkinson, and JiuJun Zhang. PEM fuel cell electrocatalysts based on transition metal macrocyclic compounds. *Coordination Chemistry Reviews*, 315:153–177, may 2016.
- [13] Robert F Service. Chemistry. Newcomer heats up the race for practical fuel cells. *Science (New York, N.Y.)*, 303(5654):29, jan 2004.
- [14] Naseam H Jafri and Sushma Gupta. Technical viability study of fuel cell as an alternative to diesel in Diesel Electric Multiple Units (DEMUs) for suburban rail transportation. In *2017 International Conference on Signal Processing and Communication (ICSPC)*, pages 181–185. IEEE, jul 2017.
- [15] Andreas Hoffrichter, Peter Fisher, Jonathan Tutcher, Stuart Hillmansen, and Clive Roberts. Performance evaluation of the hydrogen-powered prototype locomotive ‘Hydrogen Pioneer’. *Journal of Power Sources*, 250:120–127, mar 2014.
- [16] Andreas Institution of Engineering and Technology., Stuart Hillmansen, and Clive Roberts. *IET electrical systems in transportation.*, volume 6. IET Research Journals, jun 2016.
- [17] D. Guida and M. Minutillo. Design methodology for a PEM fuel cell power system in a more electrical aircraft. *Applied Energy*, 192:446–456, apr 2017.
- [18] Bulent Sarlioglu and Casey T. Morris. More Electric Aircraft: Review, Challenges, and Opportunities for Commercial Transport Aircraft. *IEEE Transactions on Transportation Electrification*, 1(1):54–64, jun 2015.
- [19] Robbert Kivits, Michael B. Charles, and Neal Ryan. A post-carbon aviation future: Airports and the transition to a cleaner aviation sector. *Futures*, 42(3):199–211, apr 2010.
- [20] Jianglan Shui, Min Wang, Feng Du, and Liming Dai. N-doped carbon nanomaterials are durable catalysts for oxygen reduction reaction in acidic fuel cells. *Science advances*, 1(1):e1400129, feb 2015.
- [21] Raymond J Gorte. Cooling down ceramic fuel cells. *Science*, 349(6254):1290–1290, sep 2015.

- [22] a. I. Baranov. Crystals with disordered hydrogen-bond networks and superprotonic conductivity. Review. *Crystallography Reports*, 48(6):1012–1037, nov 2003.
- [23] T. Rhimi, G. Leroy, B. Duponchel, K. Khirouni, S. Guermazi, and M. Toumi. Electrical conductivity and dielectric analysis of NaH₂PO₄ compound. *Ionics*, 24(11):3507–3514, nov 2018.
- [24] Anna A. Gaydamaka, Valentina G. Ponomareva, and Irina N. Bagryantseva. Rb₅H₇(PO₄)₄ as a new example of the superprotonic conductor. *Ionics*, pages 1–7, dec 2018.
- [25] Saloua Belghith, Yahya Bahrouni, and Latifa Ben Hamada. Synthesis, Crystal Structure and Characterization of a New Dihydrogenomonophosphate: (C₇H₉N₂O)H₂PO₄. *Open Journal of Inorganic Chemistry*, 05(04):122–130, aug 2015.
- [26] Yuya Yoshii, Norihisa Hoshino, Takashi Takeda, and Tomoyuki Akutagawa. Protonic Conductivity and Hydrogen Bonds in (Haloanilinium)(H₂PO₄) Crystals. *The Journal of Physical Chemistry C*, 119(36):20845–20854, sep 2015.
- [27] Sang-Hyung Lee, Sung-Tae Lee, Dae-Han Lee, Sang-Min Lee, Sang-Soo Han, and Sung-Ki Lim. CsHSO₄/TiP₂O₇ composite membrane for high temperature (> 150° C) proton exchange membrane fuel cells. *International Journal of Hydrogen Energy*, 40(37):12770–12775, oct 2015.
- [28] H. Litaïem, S. Garcia-Granda, L. Ktari, and M. Dammak. The structural behaviour before the ionic–protonic superconduction phase transition and thermal properties in the caesium sulphate arsenate tellurate compound. *Journal of Thermal Analysis and Calorimetry*, 123(1):391–400, jan 2016.
- [29] Matthias Weil. Insights into Formation Conditions, Crystal Structures, and Thermal Behavior of Hydrous and Anhydrous Barium Arsenates. *Crystal Growth & Design*, 16(2):908–921, feb 2016.
- [30] Chisholm and Haile. Structure and thermal behavior of the new superprotonic conductor Cs₂(HSO₄)(H₂PO₄). *Acta crystallographica. Section B, Structural science*, 55(Pt 6):937–946, dec 1999.
- [31] E. Ortiz, R. A. Vargas, J. C. Tróchez, J. Bornacelli, and H. Núñez. On the novel superprotonic conductor material β -Cs₃(HSO₄)₂[H_{2-x}(P_{1-x}S_x)O₄](x = 0.5): Does it behave as a solid phase? *physica status solidi (c)*, 4(11):4070–4074, nov 2007.

- [32] Sossina M Haile, Pamela M Calkins, and Dane Boysen. Superprotonic conductivity in β -Cs₃(HSO₄)₂(H_x(P,S)O₄). *Solid State Ionics*, 97(1-4):145–151, may 1997.
- [33] M. Boubia, M. T. Averbuch-Pouchot, and A. Durif. Ordered AsO₄ and SO₄ tetrahedra in diammonium trihydrogenarsenate sulfate. *Acta Crystallographica Section C Crystal Structure Communications*, 41(11):1562–1564, nov 1985.
- [34] K. Ghorbel, H. Litaïem, L. Ktari, S. Garcia-Granda, and M. Dammak. Ionic-protonic conduction analysis and dielectric relaxation behavior of the rubidium ammonium arsenate tellurate. *Ionics*, 22(2):251–260, aug 2015.
- [35] Irina Makarova, Vadim Grebenev, Elena Dmitricheva, Ilya Vasiliev, Vladimir Komornikov, Valentina Dolbinina, and Alexey Mikheykin. MmHn(XO₄)(m + n)/2 crystals: structure, phase transitions, hydrogen bonds, conductivity. II. Structure and properties of Cs₃ (HSO₄)₂(H₂ PO₄) and Cs₄(HSO₄)₃(H₂PO₄) single crystals. *Acta Crystallographica Section B Structural Science, Crystal Engineering and Materials*, 72(1):133–141, feb 2016.
- [36] N. Nouiri, K. Jaouadi, T. Mhiri, and N. Zouari. Structure, thermal behavior, and dielectric properties of new cesium hydrogen sulfate arsenate: Cs₂(HSO₄)(H₂AsO₄). *Ionics*, 22(9):1611–1623, sep 2016.
- [37] Geletu Qing and Ryuji Kikuchi. Interfacial interaction and melting point depression of CsH₅(PO₄)₂ in CsH₅(PO₄)₂/SiO₂ composites. *Solid State Ionics*, 289:133–142, jun 2016.
- [38] Ayako Ikeda, Daniil A. Kitchaev, and Sossina M. Haile. Phase behavior and superprotonic conductivity in the Cs 1- x Rb x H 2 PO 4 and Cs 1- x K x H 2 PO 4 systems. *J. Mater. Chem. A*, 2(1):204–214, nov 2014.
- [39] V. G. Ponomareva, V. V. Martsinkevich, and Yu. A. Chesalov. Transport and thermal characteristics of Cs 1- x Rb x H 2 PO 4. *Russian Journal of Electrochemistry*, 47(5):605–612, may 2011.
- [40] E. V. Selezneva, I. P. Makarova, V. V. Grebenev, and V. A. Komornikov. The Influence of Cation Substitution on the Kinetics of Phase Transitions in Crystals of (K,NH₄)₃H(SO₄)₂ Solid Solutions. *Crystallography Reports*, 63(2):178–185, 2018.

- [41] Ł. Lindner, M. Zdanowska-Frączek, A. Pawłowski, and Z.J. Frączek. Impedance spectroscopy study of $(\text{NH}_4)_3\text{H}(\text{SeO}_4)_2$: Evidence of increase in lattice disorder in the low temperature phases. *Solid State Ionics*, 311:26–30, nov 2017.
- [42] Junko Hatori, Yasumitsu Matsuo, and Seiichiro Ikehata. The relation between elasticity and the superprotonic phase transition temperature for $\text{M}_3\text{H}(\text{XO}_4)_2$. *Solid State Communications*, 140(9-10):452–454, dec 2006.
- [43] J. Wolak, A. Pawlowski, M. Polomska, and A. Pietraszko. Molecular dynamics in $(\text{NH}_4)_3\text{H}(\text{SeO}_4)_2$ at superionic phase transitions: Raman spectroscopy study. *Phase Transitions*, 86(2-3):182–190, feb 2013.
- [44] Antoni Pawłowski, Maria Połomska, Bożena Hilczer, Ludwik Szcześniak, and Adam Pietraszko. Superionic phase transition in $\text{Rb}_3\text{D}(\text{SeO}_4)_2$ single crystals. *Journal of Power Sources*, 173(2):781–787, nov 2007.
- [45] Fumihito Shikanai, Keisuke Tomiyasu, Naofumi Aso, Shinichi Itoh, Susumu Ikeda, Takashi Kamiyama, Shinya Tsukada, Jun Kano, and Seiji Kojima. Dynamical Properties of Protonic Conductor $\text{K}_3\text{H}(\text{SeO}_4)_2$. *Ferroelectrics*, 416(1):101–107, jan 2011.
- [46] Fumihito Shikanai, Shinya Tsukada, Jun Kano, and Seiji Kojima. Acoustic phonons and a central mode in the protonic conductor $\text{K}_3\text{H}(\text{SeO}_4)_2$. *Physical Review B*, 81(1):012301, jan 2010.
- [47] A Pawlowski. Pretransitional effects at the superionic phase transition of $\text{Rb}_3\text{H}(\text{SeO}_4)_2$ protonic conductor. *Solid State Ionics*, 157(1-4):203–208, feb 2003.
- [48] Y MATSUO, J HATORI, and S IKEHATA. Spin-lattice relaxation below superprotonic phase transition in $\text{Rb}_3\text{H}(\text{SeO}_4)_2$. *Solid State Ionics*, 178(7-10):671–673, apr 2007.
- [49] R.H. Chen, R.Y. Chang, and S.C. Shern. Dielectric and AC ionic conductivity investigations in $\text{K}_3\text{H}(\text{SeO}_4)_2$ single crystal. *Journal of Physics and Chemistry of Solids*, 63(11):2069–2077, nov 2002.
- [50] Abdul W. Al-Kassab, John Liesegang, and Bruce D. James. Vibrational spectroscopic, conductivity, and calorimetric studies on tripotassium hydrogen diselenate. *Structural Chemistry*, 4(1):19–22, feb 1993.

- [51] A. I. Baranov, B. V. Merinov, A. B. Tregubchenko, L. A. Shuvalov, and N. M. Shchagina. Phase transitions, structure, protonic conductivity and dielectric properties of $\text{Cs}_3\text{H}(\text{SeO}_4)_2$ and $\text{Cs}_3(\text{H, D})(\text{SeO}_4)_2$. *Ferroelectrics*, 81(1):187–191, may 1988.
- [52] A. A. Simonov, I. P. Makarova, and V. V. Grebenev. Structural mechanisms of proton conduction in $\text{Me}_m\text{H}_n(\text{XO}_4)_{(m+n)/2}$ crystals. *Physics of the Solid State*, 51(8):1566–1569, aug 2009.
- [53] L COWAN, R MORCOS, N HATADA, A NAVROTSKY, and S HAILE. High temperature properties of $\text{Rb}_3\text{H}(\text{SO}_4)_2$ at ambient pressure: Absence of a polymorphic, superprotonic transition. *Solid State Ionics*, 179(9-10):305–313, may 2008.
- [54] Calum R.I. Chisholm and Sossina M. Haile. High-temperature phase transitions in $\text{K}_3\text{H}(\text{SO}_4)_2$. *Solid State Ionics*, 145(1-4):179–184, dec 2001.
- [55] R.H. Chen, R.Y. Chang, C.S. Shern, and T. Fukami. Structural phase transition, ionic conductivity, and dielectric investigations in $\text{K}_3\text{H}(\text{SO}_4)_2$ single crystals. *Journal of Physics and Chemistry of Solids*, 64(4):553–563, apr 2003.
- [56] M. Połomska, L. F. Kirpichnikova, T. Pawłowski, and B. Hilczer. Ferroelasticity of $\text{M}_3\text{H}(\text{XO}_4)_2$ Crystals: FT NIR Raman, Ferroelastic Domain and Pretransitional Effects Studies. *Ferroelectrics*, 290(1):51–59, jan 2003.
- [57] M. Ichikawa, T. Gustafsson, and I. Olovsson. Linear relation between transition temperature and H-bond distance in $\text{M}_3\text{H}(\text{SeO}_4)_2$ -type crystals ($\text{M} = \text{K, Rb, Cs}$) with 0-dimensional H-bond network. *Solid State Communications*, 87(4):349–353, jul 1993.
- [58] A. Devendar Reddy, S.G. Sathyanarayan, and G. Sivarama Sastry. Proton conduction in $(\text{NH}_4)_3\text{H}(\text{SO}_4)_2$ single crystals. *Solid State Communications*, 43(12):937–940, sep 1982.
- [59] Takuo Ito and Hiroshi Kamimura. New Mechanism of Ionic Conductivity in Hydrogen-Bonded Crystals $\text{M}_3\text{H}(\text{XO}_4)_2$ [$\text{M}=\text{Rb, Cs, X}=\text{S, Se}$]. *Journal of the Physics Society Japan*, 67(6):1999–2007, jun 1998.
- [60] Natalie I Pavlenko. Protonic conductivity at the superionic phase transitions in the $\text{M}_3\text{H}(\text{XO}_4)_2$ crystal group. *Journal of Physics: Condensed Matter*, 11(26):5099–5110, jul 1999.

- [61] Fumihito Shikanai, Keisuke Tomiyasu, Naofumi Aso, Susumu Ikeda, and Takashi Kamiyama. Dynamical behavior of SeO_4 tetrahedra in protonic conductor $\text{K}_3\text{H}(\text{SeO}_4)_2$. *Physical Review B*, 80(14):144103, oct 2009.
- [62] Yukihiro Yoshida, Junko Hatori, Hinako Kawakami, Yasumitsu Matsuo, and Seiichiro Ikehata. Flexibility of Hydrogen Bond and Lowering of Symmetry in Proton Conductor. *Symmetry*, 4(4):507–516, aug 2012.
- [63] A. Gordon. Influence of phase transitions on the ionic conductivity of protonic superconductors. *Physical Review B*, 52(10):R6999–R7001, sep 1995.
- [64] Dalibor Merunka and Boris Rakvin. Mechanism of quantum effects in hydrogen-bonded crystals of the $\text{K}_3\text{H}(\text{SO}_4)_2$ group. *Physical Review B*, 79(13):132108, apr 2009.
- [65] N. Pavlenko, A. Pietraszko, A. Pawlowski, M. Polomska, I. V. Stasyuk, and B. Hilczer. Hydrogen transport in superionic system $\text{Rb}_3\text{H}(\text{SeO}_4)_2$: A revised cooperative migration mechanism. *Physical Review B*, 84(6):064303, aug 2011.
- [66] Koh-ichi Suzuki and Shigenobu Hayashi. ^1H NMR study of proton dynamics in the inorganic solid acid $\text{Rb}_3\text{H}(\text{SO}_4)_2$. *Physical Review B*, 73(2):024305, jan 2006.
- [67] W. Bednarski, A. Ostrowski, and S. Waplak. EPR evidence of local lattice mode in $\text{K}_3\text{H}(\text{SO}_4)_2$ and $\text{Rb}_3\text{H}(\text{SO}_4)_2$ fast-proton conductors. *Solid State Communications*, 146(9-10):365–367, jun 2008.
- [68] Y.J. Sohn, K.M. Sparta, M. Meven, G. Roth, and G. Heger. Superprotonic conductivity of $(\text{NH}_4)_3\text{H}(\text{SO}_4)_2$ in the high-temperature phase. *Solid State Ionics*, 252:116–120, dec 2013.
- [69] I. P. Makarova, T. S. Chernaya, A. A. Filaretov, A. L. Vasil'ev, I. A. Verin, V. V. Grebenev, and V. V. Dolbinina. Investigation of the structural conditionality for changes in physical properties of $\text{K}_3\text{H}(\text{SO}_4)_2$ crystals. *Crystallography Reports*, 55(3):393–403, may 2010.
- [70] I. P. Mkarova, L. A. Shuvalov, and V. I. Simonov. Structural phase transitions in $\text{Rb}_3\text{H}(\text{SeO}_4)_2$ single crystals. *Ferroelectrics*, 79(1):111–116, feb 2011.
- [71] O. S. Hernández-Daguer, H. Correa, and R. A. Vargas. Phase behaviour and superionic phase transition in $\text{K}_3\text{H}(\text{SeO}_4)_2$. *Ionics*, 21(8):2201–2209, aug 2015.

- [72] Kwang-Sei Lee. Hidden nature of the high-temperature phase transitions in crystals of KH_2PO_4 -TYPE : Is it a physical change ? *Journal of Physics and Chemistry of Solids*, 57(3):333–342, mar 1996.
- [73] O. Hernández, J. Bornacelli, M. Díaz, E. Chávez, J. C. Tróchez, and E. Ortiz. Efecto del Tamaño de Grano Sobre las Transiciones de Fase Ortorrombica, Tetragonal y Tetragonal Cubica en Titanato de Bario. *Revista de la Sociedad Colombiana de Física*, 41(1):37–39, 2009.
- [74] J Liesegang A.W Al-kassab, B.D James. Differential scanning calorimetric and electrical conductivity measurement on superionic $\text{Rb}_4\text{H}_2(\text{SeO}_4)_3$. *Journal of Physics and Chemistry of Solids*, 54(4):439–443, apr 1993.
- [75] Bożena Hilczer, Maria Połomska, and Antoni Pawłowski. Structural relaxation in superprotonic tetraammonium dihydrogen triselenate single crystals. *Solid State Ionics*, 125(1-4):163–169, oct 1999.
- [76] A. Pawłowski, B. Hilczer, M. Połomska, and A. Pietraszko. Low-temperature behaviour of $(\text{NH}_4)_4\text{H}_2(\text{SeO}_4)_3$ and $(\text{ND}_4)_4\text{D}_2(\text{SeO}_4)_3$ superionic conductors. *Solid State Ionics*, 145(1-4):217–224, dec 2001.
- [77] M. Połomska and J. Wolak. NIR Raman studies of molecular dynamics in superionic $(\text{NH}_4)_4\text{H}_2(\text{SeO}_4)_3$. *Journal of Molecular Structure*, 555(1-3):139–148, nov 2000.
- [78] T. Fukami and R.H. Chen. Refinement of Crystal Structures at Room Temperature and Structural Phase Transitions for $(\text{NH}_4)_4\text{H}_2(\text{SeO}_4)_3$ and $(\text{ND}_4)_4\text{D}_2(\text{SeO}_4)_3$ Crystals. *physica status solidi (b)*, 214(2):219–227, aug 1999.
- [79] M. A. Augustyniak and S. K. Hoffmann. Non-stoichiometry effects in the properties of $(\text{NH}_4)_3\text{H}(\text{SeO}_4)_2$ and $(\text{NH}_4)_4\text{H}_2(\text{SeO}_4)_3$ crystals. Dielectric and ESR studies. *Ferroelectrics*, 132(1):129–139, jul 1992.
- [80] Carl Henrik Görbitz. What is the best crystal size for collection of X-ray data? Refinement of the structure of glycyl- L -serine based on data from a very large crystal. *Acta Crystallographica Section B Structural Science*, 55(6):1090–1098, dec 1999.
- [81] George M Sheldrick. A short history of SHELX. *Acta crystallographica. Section A, Foundations of crystallography*, 64(Pt 1):112–22, jan 2008.

- [82] Leonard J Barbour. X-Seed – A Software Tool for Supramolecular Crystallography. *Journal of Supramolecular Chemistry*, 1(4-6):189–191, jul 2001.
- [83] Jenny Pickworth Glusker and Kenneth N. Trueblood. *Crystal Structure Analysis: A Primer*. INTERNATIONAL UNION OF CRYSTALLOGRAPHY BOOK SERIES, 3rd edition, 1998.
- [84] J. Baran, T. Lis, M. Marchewka, and H. Ratajczak. Structure and polarized IR and Raman spectra of $\text{Na}_2\text{SeO}_4 \cdot \text{H}_2\text{SeO}_3 \cdot \text{H}_2\text{O}$ crystal. *Journal of Molecular Structure*, 250(1):13–45, oct 1991.
- [85] Louis J. Farrugia. WinGX and ORTEP for Windows : an update. *Journal of Applied Crystallography*, 45(4):849–854, aug 2012.
- [86] Team The POV-Ray. POV-Ray- Persistence of Vision Raytracer, 2000.
- [87] A. Kálmán, J. S. Stephens, and D. W. J. Cruickshank. The crystal structure of K_2SeO_4 . *Acta Crystallographica Section B Structural Crystallography and Crystal Chemistry*, 26(10):1451–1454, oct 1970.
- [88] George A. Jeffrey. *An Introduction to Hydrogen Bonding*, volume 76. American Chemical Society, New York, jun 1999.
- [89] A. F. Wells and M. Bailey. 278. The structures of inorganic oxy-acids: the crystal structure of selenious acid. *Journal of the Chemical Society (Resumed)*, pages 1282–1288, jan 1949.
- [90] I. Takahashi, A. Onodera, and Y. Shiozaki. Structure of rubidium selenate at room temperature. *Acta Crystallographica Section C Crystal Structure Communications*, 43(2):179–182, feb 1987.
- [91] F. Krebs Larsen, M. S. Lehmann, Inger Søtofte, P. Beronius, Jan E. Engebretsen, and L. Ehrenberg. A Neutron Diffraction Study of Selenious Acid, H_2SeO_3 . *Acta Chemica Scandinavica*, 25:1233–1240, 1971.
- [92] Stephan Pollitt and Matthias Weil. Polymorphism of H_2SeO_3 , NaHSO_4 and $\text{Na}_5\text{H}_3(\text{SeO}_4)_4(\text{H}_2\text{O})_2$, and Re-refinement of the Crystal Structure of $\text{Te}_2\text{O}_4(\text{OH})_2$. *Zeitschrift für anorganische und allgemeine Chemie*, 640(8-9):1622–1631, jul 2014.
- [93] J. Scarlato, E.A.; Higa. SELENIUM (PIM 483).

6 Appendix

Table 9: Symmetry transformations used to generate equivalent atoms

#1 $x, -y+3/2, -z+1$	#2 $-x+2, -y+1, -z+1$	#3 $-x+2, y+1/2, z$
#4 $x, y+1, z$	#5 $x, y, -z+1/2$	#6 $-x+1, -y+1, z-1/2$
#7 $-x+1, -y+1, -z+1$	#8 $x, -y+1/2, -z+1$	#9 $-x+1, y-1/2, z$
#10 $-x+2, y-1/2, z$	#11 $x, y, -z+3/2$	#12 $x+1, -y+3/2, -z+1$
#13 $-x+2, y-1/2, -z+3/2$	#14 $-x+2, -y+1, z+1/2$	#15 $x-1, -y+3/2, -z+1$